

Comparison of Direct Collocation Optimal Control to Trajectory Optimization for Parameter Identification of an Ellipsoidal Foot-Ground Contact Model

Mahdokht Ezati · Peter Brown · Bornha Ghannadi · John McPhee

Received: date / Accepted: date

Abstract Foot-ground contact models play an important role in the accuracy of predictive human gait simulations, and there is a need for a computationally-efficient dynamic contact model for predictive and evaluative studies. In this research, we generated symbolic dynamic equations for a 2D torque-driven 11-DOF human model with a 3D ellipsoidal volumetric foot-ground contact model. The main goal was to increase the prediction accuracy and decrease the computation time for human gait analyses compared to the previous studies that used numerical formulations and point foot-ground contact models.

A data-tracking optimization was developed to identify the contact parameters of the human gait model using two optimization approaches: trajectory optimization and optimal control. The first approach is developed with a global search algorithm based on inverse dynamics. In this algorithm, a local optimizer is repeatedly run from multiple potential start points to select the best start point while satisfying the constraints and reaching the lowest cost function value. The second approach is developed using direct collocation based on implicit dynamics. In this method, the optimization problem is solved using a variable-order adaptive orthogonal collocation method along with sparse nonlinear programming.

Optimal control was superior to trajectory optimization for identifying a large number of parameters; the simulated torques and ground reaction forces from the optimal control correlated better with the experimental data. For the optimal control, the root-mean-square errors of the resultant torques, tangential and normal ground reaction forces were 0.48 (N.m), 14.07 (N) and 26.44 (N), respectively. However, for the trajectory optimization, these errors were 15.19 (N.m), 36.51 (N) and 234.57 (N). Thus, the optimized contact

M. Ezati
Systems Design Engineering, University of Waterloo, Waterloo, ON, Canada
E-mail: mezati@uwaterloo.ca

P. Brown
Systems Design Engineering, University of Waterloo, Waterloo, ON, Canada
E-mail: pm2brown@uwaterloo.ca

B. Ghannadi
MapleSoft Inc., Waterloo, ON, Canada
E-mail: bghannadi@maplesoft.com

J. McPhee
Systems Design Engineering, University of Waterloo, Waterloo, ON, Canada
E-mail: mcphee@uwaterloo.ca

model from the optimal control, which was developed symbolically and based on volumetric contact equations, is a suitable foot-ground contact model for predictive human gait simulations. Additionally, we demonstrated that optimal control could be used to predict the motion and torque for the metatarsal joints, which are not easily measurable in practice.

Keywords Ellipsoidal volumetric contact · Foot-ground contact · Human gait simulation · Contact parameter identification · Direct collocation · Trajectory optimization

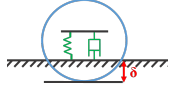
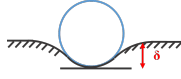
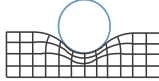
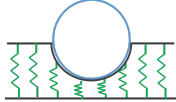
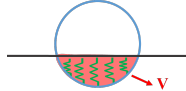
1 Introduction

Predictive human task simulation is an interesting area of research due to its application in evaluative studies (e.g., model-based assistive device controllers [11], surgical intervention planning [41], athletic training [34], prosthesis and orthosis design [42,43]). Among human tasks, gait is one of the most complicated and as a consequence, its predictive simulation is challenging due to its highly nonlinear motion equations, nonlinear muscle dynamics, and nonlinear foot-ground contact model.

The foot-ground contact can be modeled as kinematic constraints that restrict the motion of discrete points along the bottom of the foot [1,19,21]. In these studies, the complex geometry of foot is not required to be explicitly modeled since a number of discrete points can approximately represent the complexity of the foot geometry. However, To achieve a useful predictive human gait simulation, it is important to have an accurate foot-ground contact model which is consistent with the complex geometry of foot and computationally efficient. The main types of contact models commonly used in biomechanics studies include point contact, finite element contact, elastic foundation contact, surrogate contact, and volumetric contact:

- Point contact models are relatively simple and assume that contact between two surfaces occurs at a point. Two different methods for point contact, Kelvin-Voigt and Hunt-Crossley [16], are illustrated in Table 1 (No. 1 and 2). In the first method, the transition between the contact and non-contact conditions is not continuous due to the linear damper. The second method does not suffer from this discontinuity [10]. However, these two point contact models may not be accurate enough for conforming surfaces.
- Finite element contact models [47] can provide a more detailed contact for complex shapes (No. 3 in Table 1). However, this is not suitable for biomechanics optimizations or real-time analysis due to the high computational time of finite element analyses.
- In elastic foundation contact models [9], the contact surface is discretized into a finite number of springs. In other words, the bottom of the foot is modeled using a set of discrete viscoelastic elements with Coulomb friction [31,33]. No. 4 in Table 1 shows the schematic of the elastic foundation contact model.
- Surrogate contact models [20] are computationally efficient in comparison to finite element models and elastic foundation models since they are developed based on lookup tables rather than physical models. Surrogate models are trained to match results from a high-fidelity model. However, they are only appropriate over the conditions for which they have been trained.
- Volumetric contact model [14] is based on the concept of an elastic foundation model, but the contact surface is modeled using a continuous collection of springs. Thus, it would be more realistic than the elastic foundation model to model complex conforming

Table 1: Contact models

No.	method	model	formula
1	Kelvin-Voigt		$F_n = k\delta + d\dot{\delta}$
2	Hunt-Crossley		$F_n = a\delta^n + (b\dot{\delta}^n)\dot{\delta}$
3	finite element		partial differential equations for each element
4	elastic foundation		discrete force equation at each spring element
5	volumetric contact		$F_n = k_V V(1 + a_V v_{cn})$

F_n is the normal contact force. δ is the penetration of deformation depth. k and d are the spring and damping constants, respectively. a and n are constants dependent on material properties and b is the damping coefficient. k_V and a_V are the volumetric stiffness and damping constants, respectively. Also, V is the volume of penetration and v_{cn} is the relative velocity of the two surfaces.

surfaces (e.g., foot). No. 5 in Table 1 shows the schematic of the model and the equation for the normal contact force.

The application of these five contact models to biomechanical modelings has been compared in detail in two review papers [12,40] to which readers are directed for more information.

Some recent gait studies, instead of using volumetric contact equations, modeled the complex geometry of the foot by a large number of spheres or ellipsoids to estimate the penetration depth for Hunt-Crossley equations. This method can be called Hunt-Crossley spherical/ellipsoidal contact model. Lin and Pandy [22], Lin et al. [23], and Porsa et al. [34] utilized this method by modeling the foot-ground contact via six, six and eight spheres, respectively. Lopes et al. [24] have also used six ellipsoids on the sole to model the foot-ground contact. For a conforming surface like a foot, Hunt-Crossley spherical/ellipsoidal contact models are more accurate than the point contact models since the penetration depth is estimated using spheres or ellipsoids. However, the volumetric contact models, in which a volume of penetration is used in the contact equations, can provide a better geometric representation of a conforming surface than Hunt-Crossley spherical contact models. Hunt-Crossley equations are most accurate for point contacts, but there are likely errors when applied to a conforming surface.

Meyer et al. [27] employed the elastic foundation contact using a large number of springs to approximate a continuous collection of springs. Thus, through their approach, the model

takes advantage of the accuracy of volumetric contact as well as the computational efficiency of the elastic foundation method.

In the contact models of [22–24, 27, 34], a finite number of contact points on the foot have been used. These foot-ground contact models can be assumed as multiple-point contact models, in which the normal contact force is evaluated via the depth of penetration using the Hunt-Crossley method. Since the Hunt-Crossley method is restricted to the contact points (not the contact surfaces), an unnatural foot shape may be obtained. However, a Hunt-Crossley ellipsoidal contact model [24] is geometrically more natural than the other multiple-point contact models.

Since the volumetric contact model provides a better representation of conforming geometry in comparison to the point contact and elastic foundation models, some human gait studies employed it to simulate the foot-ground contact. The common type of volumetric contact model, generally used for foot-ground contact, is the spherical volumetric contact model. Millard et al. [28] used a 2D two-segment foot model with three volumetric sphere-plane contact pairs. Shourijeh et al. [39, 38] developed that model into a hyper-volumetric model. Mouzo et al. [30] also employed volumetric contact with a polynomial representing the contact surface.

Brown and McPhee [5] have developed an ellipsoidal volumetric foot-ground contact model that takes advantage of the features of ellipsoidal models and volumetric models. In their approach, the foot is modeled by three ellipsoids and the volumetric contact equations for an ellipsoid contacting a plane were employed. Since ellipsoids can match the complex geometry of the foot surface better than spheres, they used only three ellipsoids to model the foot-ground contact. However, there still exist some gaps in Brown and McPhee's approach that should be filled before being used in high fidelity human gait analyses.

The first gap is that the contact parameters have been identified by tracking the experimental foot-ground reactions (i.e., the normal force, center of pressure and pressure at the foot surface) measured for one foot during gait. Not only did they not include both feet in the identification process, but they did not also consider the dynamics of the lower extremities.

The second gap is that once they included friction in their model, the contact parameter identification yielded inaccurate parameters and results. This gap is due to using a continuous velocity-based friction model in an inverse dynamic identification.

The main contribution of this paper is to fill in these gaps of the ellipsoidal volumetric contact model, so that it may be used as a computational-efficient and accurate foot-ground contact model in predictive gait simulations. To this end, a 2D human model with lower extremities was developed and the 3D ellipsoidal volumetric contact was applied on both feet. To increase the accuracy and computational efficiency, the dynamic equations of the multibody model were developed symbolically. Two approaches were used to identify the contact parameters by tracking not only the experimental foot-ground reactions but also the kinematics and dynamics of the lower extremities: Trajectory optimization and optimal control. The contact parameters can be identified for a 3D volumetric contact model although the human model is 2D. The reason is that the natural waking task is mainly done by humans in the sagittal plane. Thus, we can restrict our study to a 2D human model in order to simplify the dynamic equations while identifying the contact parameters for a general 3D ellipsoidal volumetric foot-ground contact model.

The trajectory optimization approach is based on inverse dynamics and the optimal control approach is based on implicit dynamic simulation (i.e., neither forward nor inverse dynamics [7]). The approaches were compared and discussed. The other contribution of this paper is that angle and torque of metatarsal joints, which are not easily measurable in

Table 2: Anthropometric data of all bodies except for the feet

body	body weight/BM	COM/body length	ROG/body length	body length/BH
HAT	0.678	0.626	0.496	0.288
thigh	0.100	0.433	0.323	0.245
shank	0.0465	0.433	0.302	0.246

practice, were calculated. To the best of the authors' knowledge, there is no human gait simulation study reporting the results of the metatarsal torque and motion even though metatarsal joints have an important role in gait analyses [8].

2 Model development

In this section, first, the human model is described and its properties are specified. Then, the foot-ground contact model is briefly explained and the contact parameters, which will be identified in Sect. 4, are introduced. Finally, the method to extract the symbolic dynamic equations of the model is defined.

2.1 Human model

The human model is a 2D torque-driven model that moves in the sagittal plane. It includes 9 bodies and 11 degrees of freedom (DOFs). The bodies are head-arms-trunk (HAT), thighs, shanks, hind-fore-feet, and toes. The DOFs are 3-DOF HAT-to-ground joint, 1-DOF hip joints, 1-DOF knee joints, 1-DOF ankle joints, and 1-DOF metatarsal joints. The schematic of the human model is shown in Fig. 1. The global coordinate system (GCS) is assumed to be fixed to the ground exactly under the center of mass of HAT at the start of simulation. Axes X , Y and Z are in the longitudinal, vertical, and lateral directions, respectively (as shown in Fig. 1).

It is a common approach to assume head, arms and trunk as a single body (HAT) in human gait analyses [29,42,43,38], since the effects of suppressing the arm swing on the kinematics, kinetics, and energetics of human gait are less than 10% [45].

The anthropometric data of the HAT, thighs and shanks were extracted from [46] and given in Table 2. In this table, BM and BH are the mass and height of the equivalent human body, respectively. COM is the center of mass position of the body, measured from the proximal head of the body. ROG is the radius of gyration around the COM and is used to calculate the moment of inertia (MOI) of the body.

For the feet, reference [46] has only reported the mass and length of the whole foot which are 0.0145BM and 0.152BH , respectively. There is no conventional anthropometric data for each foot segment in the literature. The weights, COMs, and ROGs of foot segments were estimated, consistent with the foot properties in [6,36] and the foot segment lengths were calculated based on the optimized foot geometry presented in [37]. The foot segment properties were scaled by BM and BH, shown in Table 3. Angle β in the picture inside Table 3 is the fixed angle between the fore-foot (AM) and the hind-foot (HA) and it was set to 106° similar to the angle employed in [37].

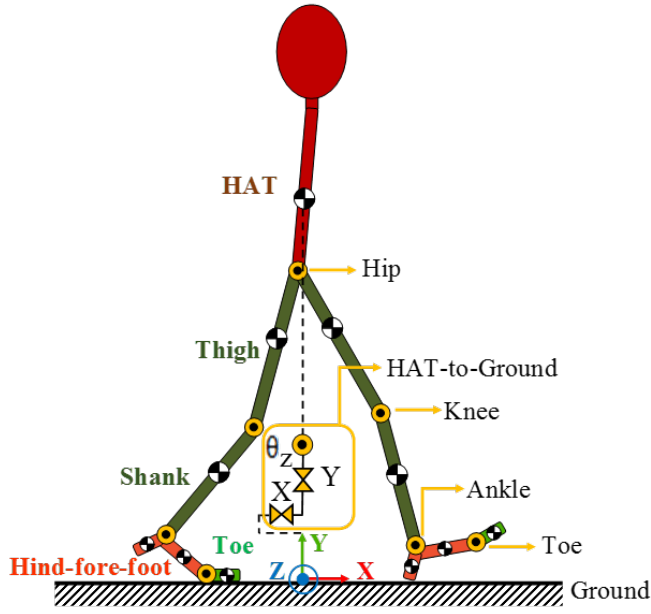
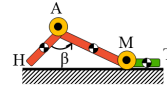


Fig. 1: 2D human model with nine bodies and eleven DOFs

Table 3: Anthropometric data of the feet

segment	body weight/BM	COM/body length	ROG/body length	body length/BH
MT	2.1e-3	0.5	1.32e-2	4.3e-2
AM	6.2e-3	0.5	2.74e-2	6.5e-2
HA	6.2e-3	0.5	2.74e-2	4.4e-2



2.2 Foot-ground contact model

To model the foot-ground contact, the most recent volumetric contact model [5] was employed, in which the contact surface has been modeled by ellipsoids and the friction has been generated by a continuous velocity-based friction model. In a velocity-based friction model, it is assumed that sticking occurs at a very small transition velocity. In this study, the transition velocity was set to 0.1 m/s, which is quite small in comparison to the experimental gait speed (1.26 m/s). Each foot is composed of two bodies: hind-fore-foot and toe. The hind-fore-foot was represented by two ellipsoids (i.e., ball and heel ellipsoids) and the toe was represented by one ellipsoid (i.e., toe ellipsoid). Fig. 2 shows an approximate schematic for the ellipsoidal contact model of the right foot. Using volumetric contact, the rolling resistance, tangential friction and spinning friction are modeled in addition to the normal force. For further information on the contact equations, readers are directed to [4, 13].

In this study, the GCS is different from that in [5]. To address this, several transformation matrices were employed to locate the ellipsoids in a correct position and orientation with respect to the GCS of this study. Additionally, in reference [5], the ellipsoidal contact model

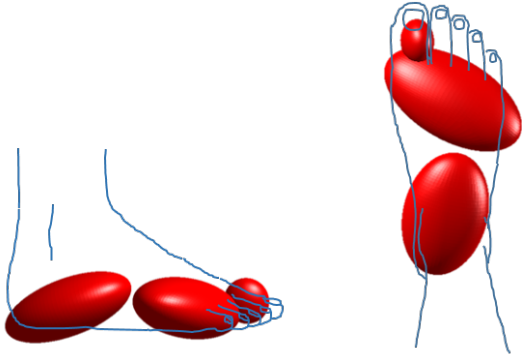


Fig. 2: Side and top views of the ellipsoidal contact model for the right foot (This figure is only for visualization purpose. The positions, orientations and dimensions of the ellipsoids are not to scale.)

Table 4: Contact model parameters

parameter	description
k_v	volumetric stiffness
a_v	volumetric damping coefficient
μ_s	static friction coefficient
μ_d	dynamic friction coefficient
a, b, c	dimensions
r_x, r_y, r_z	position
γ, β, α	3-2-1 body-fixed Euler angles

Parameters r_x , r_y and r_z specify the locations of the ellipsoid centroids with respect to the GCS; parameters γ , β and α represent 3-2-1 body-fixed Euler angles with respect to the GCS and parameters a , b and c specify the ellipsoid radii in the local x , y and z axes, respectively.

was developed only for the left foot. The three ellipsoids of the left foot were reflected with respect to the sagittal plane to develop the contact model for the right foot. Thus, six ellipsoids (three ellipsoids on each foot) were used to model the contact.

Each ellipsoid contacting a plane has 13 parameters (Table 4). Since we have three different ellipsoids (ball, heel, and toe), there are 39 parameters in total which will be identified in Sect. 4. It should be noted that the human model is bilaterally symmetric and in gait, the right and left legs perform similar motions but with a time shift. Thus, the contact parameters of ball, heel and toe ellipsoids on the left foot are assumed to be identical with those on the right foot.

2.3 Dynamics modeling

The human with foot-ground contact model was developed in MapleSim (2018. Maplesoft, Waterloo, ON, Canada), as shown in Fig. 3. An advantage of using MapleSim is that the motion dynamic equations are generated in a symbolic form; also, the velocity and acceleration equations can be directly determined by symbolically differentiating the kinematic expressions with respect to time. The resultant equations are more

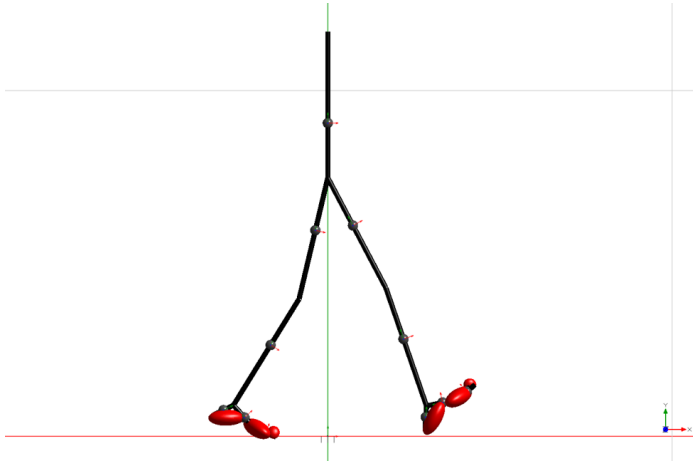


Fig. 3: Developed human model with the ellipsoidal foot-ground contact in MapleSim

computationally efficient than a numerical equivalent [26]. If the dynamic equations are evaluated numerically during the optimization, the motion equations have to be differentiated in each iteration of optimization, which leads to a more time-consuming procedure and less accurate results than the optimization in which the symbolic equations are used.

The final symbolic equations, extracted from the MapleSim model, were modified in Maple (2018 Maplesoft, Waterloo, ON, Canada) to reduce the size of the simulation code and get optimal symbolic equations for exporting to MATLAB (R2018b, Mathworks, Natick, MA, USA) for use in the optimization process.

3 Gait experiments

Experimental gait data is required for parameterizing the contact model and validating the results. To generate an accurate data-tracking optimization for this study, the motion data for all 11 DOF of the model, joint torque data for all 8 joints of the model, and normal and tangential ground reaction forces (GRFs) for both feet are used.

The experimental data processing is categorized into three subsections: (3.1) HAT and right leg without metatarsal, (3.2) Right metatarsal and (3.3) Left leg. In each subsection, it is explained in detail how the data corresponding to those specific bodies is extracted, estimated or generated.

3.1 HAT and right leg without metatarsal

The experimental position of the HAT with respect to the ground, the experimental angles and torques of right hip, knee and ankle joints and the GRFs of the right foot were extracted from [3] for one gait cycle. A gait cycle is composed of two steps and in this study assumed to start and end with the heel-strike of the right foot on the ground.

The orientation of the HAT with respect to the ground was set to zero as the initial guess for the optimization because the variation of this orientation during natural-speed

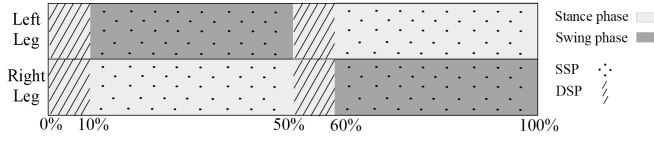


Fig. 4: Phases of right and left leg during one gait cycle starting and ending with the right heel-strike

gait is negligible ($-1^\circ \leq \theta_z \leq 1^\circ$ [46]). This angle will be predicted when the other known experimental data are tracked in the optimization.

In reference [3], 20 healthy young subjects (9 males and 11 females with an age of 10.8 ± 3.2 years, a mass of 41.4 ± 15.5 kg and a height of 1.47 ± 0.2 m) have participated. The experimental motions of the HAT, right hip, knee, and ankle have been collected for natural-speed walking using the 9-camera SMART-E motion capture system (BTS, Milano, Italy) and LAMB market set including 29 retroreflective markers. The experimental GRFs of the right foot were measured using two force plates (Kistler, Winterthur, Switzerland). The experimental torques of right hip, knee and ankle were calculated by solving the inverse dynamics problem given the experimental motion and GRFs of the right leg.

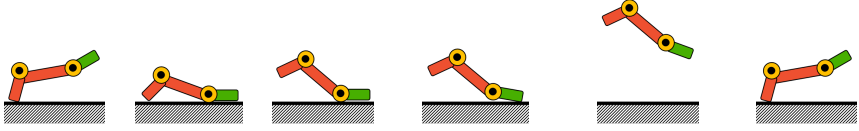
3.2 Right metatarsal

To the best of our knowledge, there is no human gait simulation study using experimentally-measured metatarsal joint data or reporting the resultant metatarsal joint motion and torque from their simulation. There are only a few clinical and laboratory studies measuring motion and pressure data for the different segments of foot (i.e. toe, fore-foot and hind-foot) during the stance phase of gait [17,18]. However, it would be unreliable to use experimentally-measured toe motion in the gait simulation studies because the rigid body assumption for the foot and marker placement during the measurement makes the toe motion data physiologically impossible for gait simulation studies. Internal movement of the foot causes this inaccuracy in the measurement [5]. Thus, for the angle of right metatarsal, We planed a meaningful trajectory using the method in [8] and considering the measured angle for the metatarsal joint in [18].

The right metatarsal motion during one gait cycle was divided into six known postures: heel-strike, toe-strike, heel-off, toe-off, toe-free and again heel-strike. Between every two subsequent postures, a 5th-order polynomial was fitted given the six known boundary conditions listed in Table 5. In this table, $\Delta \theta_a$ is the range for the ankle angle and t_{SSP} and t_{DSP} represent the duration of single-support phase (SSP) and double-support phase (DSP), respectively. During the SSP only one foot is in contact with the ground and in DSP both feet are on the ground. One gait cycle is composed of two SSPs and two DSPs. For our experimental data, each SSP and DSP are 10% and 40% of the gait cycle, respectively [3]. Fig. 4 shows these phases for both feet which are either in swing or stance phase during the gait cycle. The planned trajectory for the right metatarsal angle is shown in Fig. 5.

Table 5: Known postures for the metatarsal trajectory

heel-strike	toe-strike	heel-off	toe-off	toe-free	heel-strike
$t = 0$	$t = t_{DSP}$	$t = t_{DSP} + t_{SSP}$	$t = 1.9t_{DSP} + t_{SSP}$	$t = 2t_{DSP} + t_{SSP}$	$t = 2t_{DSP} + 2t_{SSP}$
$\theta = \theta_0$	$\theta = \theta_0$	$\theta = 0.12\Delta\theta_a$	$\theta = 0.4\Delta\theta_a$	$\theta = \theta_0$	$\theta = \theta_0$
$\dot{\theta} = 0$	$\dot{\theta} = 0$	$\dot{\theta} = 0$	$\dot{\theta} = 0$	$\dot{\theta} = 0$	$\dot{\theta} = 0$
$\ddot{\theta} = 0$	$\ddot{\theta} = 0$	$\ddot{\theta} = 0$	$\ddot{\theta} = 0$	$\ddot{\theta} = 0$	$\ddot{\theta} = 0$



θ , $\dot{\theta}$ and $\ddot{\theta}$ are the angle, angular velocity and angular acceleration of the right metatarsal, respectively. θ_0 is the metatarsal angle when the toe is free. $\Delta\theta_a$ is the variation of the ankle angle (i.e., the difference between the max and min values of ankle angle). t_{DSP} and t_{SSP} are the duration of DSP and SSP, respectively.

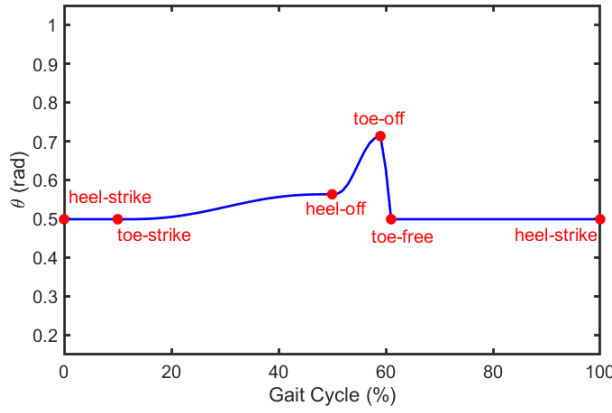


Fig. 5: The planned trajectory for the right metatarsal joint angle

3.3 Left leg

The motions of legs were assumed to be bilaterally symmetric with a time shift during a gait cycle. The time shift (T_{sh}) is equal to $t_{DSP} + t_{SSP}$ based on Fig. 4. The data of the left leg can be easily generated through the data of the right leg extracted/estimated in Sect. 3.1 and Sect. 3.2.

Since human gait is a periodic task, a Fourier series can be used to generate data for the left leg [25]. A Fourier series was fitted to the data of the right leg, with the Fourier basis signal matrix and the coefficient vector defined as:

$$[x_j]_{n \times 1} = [1 \cos(i\omega t_j) \sin(i\omega t_j)]_{n \times (1+2m)} \times \begin{bmatrix} a_0 \\ a_i \\ b_i \end{bmatrix}_{(1+2m) \times 1} \quad (1)$$

where, n and m are the number of data points and the order of the Fourier series with values of 101 and 5, respectively. Indices i and j are $i = [1, \dots, m]$ and $j = [1, \dots, n]$, respectively.

Index r refers to the right leg and x_j is the data at time instant t_j . The Fourier coefficients are a_0 , a_i and b_i . ω equals $2\pi/T_c$ in which T_c is the duration of the gait cycle.

In Eq. 1, the data and the signal matrix of the right leg are known. So, the vector of coefficients can be easily obtained. Then, a new Fourier basis signal matrix was created for the left leg:

$$M_l = [1 \cos(i\omega(t_j + T_{sh})) \sin(i\omega(t_j + T_{sh}))]_{n \times (1+2m)} \quad (2)$$

where, index l refers to the left leg. Finally, the data of the left leg can be calculated through:

$$[x_j]_{l \times n} = M_l \times [1 \cos(i\omega t_j) \sin(i\omega t_j)]_{(1+2m) \times n}^\dagger \times [x_j]_{r \times n} \quad (3)$$

where † is pseudoinverse of the matrix. This approach was used to generate all motions, torques, and GRFs of the left leg from the data of the right leg.

4 Contact parameter identification

We used two different optimization approaches (i.e., trajectory optimization and optimal control) to identify the contact parameters. These two approaches are often confused and used interchangeably [35]. In trajectory optimization, static parameter values are identified to optimize a given performance index. In contrast, in optimal control, time-variant inputs to a system and, optionally, static parameters are estimated to optimize a given performance index.

In this section, the solvers, methodologies, constraints and cost functions of the two optimization approaches, developed in MATLAB (R2018b. MathWorks, Natick, MA, USA), are explained and compared.

4.1 Trajectory optimization

4.1.1 Solver

To implement the trajectory optimization, GlobalSearch algorithm [44], a global optimization toolbox for MATLAB, was used. The GlobalSearch uses a scatter-search mechanism to generate multiple start points for sampling multiple basins of interest. Then, GlobalSearch starts a local solver (i.e., fmincon) repeatedly to analyze the start points and remove those points that can not help to find the global minimum. Finally, the best parameter set that satisfies all constraints and has the lowest cost function value is selected as the global optimization solution. In this approach, the differential equations are solved by explicitly integrating or differentiating. The flowchart of this optimization method is illustrated in Fig. 6. This optimization was done on a desktop computer with an Intel® Core™ i7-6700 CPU @ 3.40 GHz with 16.0 GB RAM.

4.1.2 Methodology

In trajectory optimization, the inverse dynamic equations of the model were explicitly solved for the joint torques and ground reaction forces and moments (GRFs) from the generalized coordinates (i.e., $q(t)$) and their derivatives (i.e., $\dot{q}(t) = v(t)$ and $\ddot{q}(t) = a(t)$). Meanwhile, the static parameters were optimized to minimize the cost function and meet

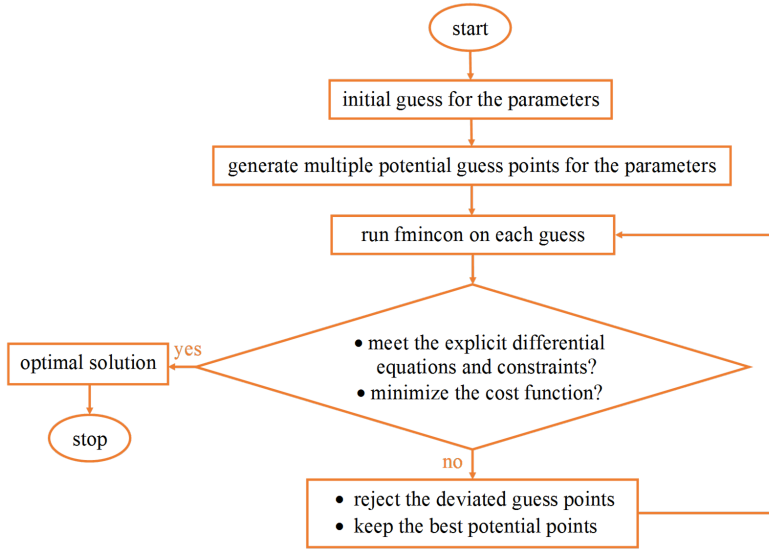


Fig. 6: The flowchart of GlobalSearch

the constraints. In this optimization, the generalized coordinates and their derivatives were set to the experimental coordinate positions, velocities, and accelerations. The static parameters, which will be identified, are the 39 contact parameters mentioned in Table 4.

4.1.3 Constraints

The dynamic friction coefficient was enforced to be less than static friction coefficient (Eq. 4):

$$\left(\frac{\mu_d}{\mu_s}\right)_{min} \leq \frac{\mu_d}{\mu_s} \leq \left(\frac{\mu_d}{\mu_s}\right)_{max} \quad (4)$$

The lower bound in Eq. 4 was set to 0.55 to prevent the model from slipping and the upper bound was set to 0.99.

4.1.4 Cost function

Experimental joint torques and GRFs were tracked over time using the following cost function:

$$J = \frac{1}{t_f} \int_{t_0}^{t_f} \left[w_1 \sum_{i=1}^6 \left(\frac{\tau_{sim.} - \tau_{exp.}}{\tau_{max} - \tau_{min}} \right)_i^2 + w_2 \sum_{j=1}^4 \left(\frac{GRF_{sim.} - GRF_{exp.}}{GRF_{max} - GRF_{min}} \right)_j^2 \right] dt \quad (5)$$

where t_0 and t_f are the initial time and final time of a gait cycle and equal to 0(s) and 0.98(s), respectively, and w_1 and w_2 are the weighting factors. Indices *sim.* and *exp.* refer to the simulation results and experimental data, respectively. τ is the torque and *GRF* includes the tangential and normal ground reaction forces. i is from 1 to 6 referring to the torques of left and right hip, knee and ankle joints. The metatarsal torques were not tracked since no

experimental data for them was available. j is from 1 to 4 referring to tangential and normal forces of the right and left feet. The minimum and maximum values of τ and GRF were obtained from the experimental data.

4.1.5 Bounds

We constrained the contact parameters to be within specified bounds. These bounds were physically-meaningful and tuned using the reported contact parameters in [5], the friction coefficients reported in [27] for the foot-ground contact, and the shape and dimensions of the human foot segments mentioned in Table 3.

The bounds were considered large enough to allow the optimization find the best parameters regarding the optimization constraints. After each optimization run, we inspected the cost function value to see whether the newly-tuned bounds bring about a lower value for the cost function than the previously-tuned bounds.

4.1.6 Initial guess

To help the optimization identify physically-meaningful values for the contact parameters, we used initial guesses for the 39 contact parameters defined in Table 4. For the volumetric stiffness, volumetric damping coefficient, the dimensions, positions and orientations of the ellipsoids, the optimal values reported in [5] were used as the initial guess. For the static and dynamic friction coefficients, 0.40 and 0.35 were assumed as the initial guess, respectively, since the required friction coefficient for walking is 0.3 [15].

4.2 Optimal control

4.2.1 Solver

To implement the optimal control algorithm, GPOPS-II [32], a direct orthogonal collocation optimal control toolbox for MATLAB, was used. In this approach, the states and control inputs are parameterized as orthogonal polynomials (in the case of a parameter identification problem, static parameters are added to the set of unknowns). The roots of those polynomials are considered as the collocation points and a local optimizer (i.e., IPOPT) updates the polynomials by increasing the number of the collocation points or displacing the collocation points until the constraints are met and the cost function is minimized regarding a prescribed error threshold. IPOPT is an interior-point optimizer where the constraints are satisfied by a barrier function. In this approach, the differential equations are considered as algebraic constraints that are satisfied during the optimization. The flowchart of this optimization method is illustrated in Fig. 7. This optimization was done on a desktop computer with an Intel® Core™ i7-6700 CPU @ 3.40 GHz with 16.0 GB RAM.

4.2.2 Methodology

In our optimal control optimization, the states and control inputs were:

$$x(t) = [q(t), v(t), a(t)] \quad (6)$$

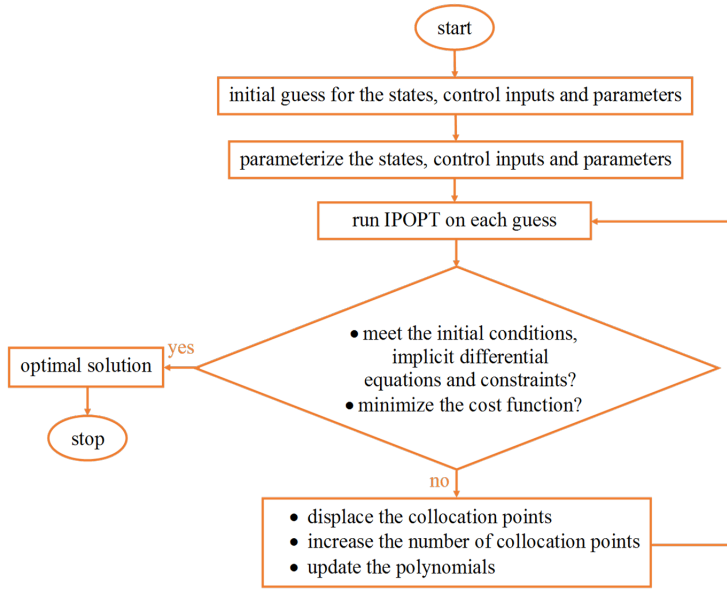


Fig. 7: The flowchart of direct orthogonal collocation

$$u(t) = [\dot{a}(t), \tau(t)] \quad (7)$$

where the states ($x(t)$) are the generalized coordinates, velocities, and accelerations. The control inputs ($u(t)$) are the joint jerks ($u_1(t) = \dot{a}(t)$) and joint torques ($u_2(t) = \tau(t)$). Considering joint jerks in addition to the joint torques as the control inputs improves convergence and solution smoothness [2]. In this optimization, the states, control inputs, and the 39 contact parameters were parameterized and then optimized to minimize a cost function subject to constraints. The dynamic equations were solved implicitly as algebraic constraints during the optimization. Implicit dynamics modeling is different from explicit forward and inverse dynamics modeling approaches [7].

For a human model with a foot-ground contact model, in the inverse approach, dynamic equations must be explicitly differentiated to estimate the joint torques and GRFMs given the motion and in the forward approach, dynamic equations must be explicitly integrated to predict the motion and GRFMs given the joint torques. Although the inverse approach is relatively fast, unrealistic joint torques may be predicted due to numerical differentiation errors and inaccurate model parameters [7]. On the other hand, the drawback of the forward approach is that explicit integration methods are time-consuming. To avoid the deficiencies of explicit inverse and forward methods, the dynamic equations are implicitly solved as an algebraic constraint; thus, this is neither a forward nor inverse dynamics modeling approaches.

4.2.3 Constraints

In addition to the constraint described for the trajectory optimization in Sect. 4.1, three extra constraints were defined for the optimal control optimization:

$$R_{min} \leq R_{pelvis} \leq R_{max} \quad (8)$$

$$\dot{x}(t) = [v(t), a(t), u_1(t)] \quad (9)$$

$$C_{min} \leq (\tau_{inv}(t) - u_2(t))^2 \leq C_{max} \quad (10)$$

In Eq. 8, the residual loads on the pelvis were imposed to be minimized to ensure dynamic consistency [27]. R represents the two residual forces and one residual moment acting on the pelvis and the bounds for the residual forces were set to -1 and 1 (N) and for the residual moment was set to -0.1 and 0.1 (N.m). Eq. 9 is the dynamic constraint which represents the first derivative of states. Eq. 10 is the algebraic constraint, in which $u_2(t)$ is the torque control inputs and τ_{inv} is the joint torques inversely obtained by solving the dynamic equations given the states. C_{min} and C_{max} were set to 0 and 10^{-12} to implicitly satisfy the motion dynamic equations.

4.2.4 Cost function

In addition to the torque-tracking and GRF-tracking cost terms, considered for the trajectory optimization in Sect. 4.1, two additional terms were included in the cost function of the optimal control optimization: a motion-tracking term and minimization of the joint jerk. These two terms cannot be used in the trajectory optimization's cost function. The reason is that, in the trajectory optimization, the kinematic inputs are constant and consequently these terms, which are kinematic-based, are always constant and cannot be minimized. The cost function of the optimal control optimization is as follows:

$$J = \frac{1}{t_f} \int_{t_0}^{t_f} \left[w_1 \sum_{i=1}^6 \left(\frac{\tau_{sim.} - \tau_{exp.}}{\tau_{max} - \tau_{min}} \right)_i^2 + w_2 \sum_{j=1}^4 \left(\frac{GRF_{sim.} - GRF_{exp.}}{GRF_{max} - GRF_{min}} \right)_j^2 + w_3 \sum_{k=1}^{11} \left(\frac{q_{sim.} - q_{exp.}}{q_{max} - q_{min}} \right)_k^2 + w_4 t_f^6 \sum_{n=1}^{11} \left(\frac{\dot{a}}{\dot{a}_{max} - \dot{a}_{min}} \right)_n^2 \right] dt \quad (11)$$

where j and n are from 1 to 11 referring to the motions and jerks of the 11 generalized coordinates, respectively. It should be noted that the jerk penalty was scaled by t_f^6 [27]. Minimizing the joint jerks results in a feasible solution even with a poor initial guess. The minimum and maximum values of motions and jerks, in the denominators, were obtained from the experimental data.

4.2.5 Bounds

In trajectory optimization, we can only define bounds for the contact parameters. In the optimal control optimization, we can define boundaries not only for the contact parameters but also for the initial and final times, states at the initial and final times, states and control inputs during the gait cycle time, and also the integrals of the cost terms. The bounds for the initial and final times were considered to be fixed and equal to 0 (s) and 0.98 (s), respectively to match the experimental gait cycle time. The bounds for the generalized coordinates at initial and final times, and the generalized coordinates and torques during the gait cycle time, were determined based on the prescribed standard deviation reported by [3]. The bounds for the contact parameters were specified and tuned by a similar approach to the one we used for the trajectory optimization. The remainder of the bounds (i.e., on the integrals, generalized velocities and accelerations at initial and final times and during the gait cycle time) were tuned regarding the experimental data.

Table 6: Weighting factor values

Optimization	Cost function	Weights
trajectory optimization	Eq. 5	$w_1 = 1/4, w_2 = 1/4$
optimal control	Eq. 11	$w_1 = 1/4, w_2 = 1/4, w_3 = 1/4, w_4 = 1/40$

Table 7: Root-mean-square errors for the trajectory optimization and optimal control

Optimization	τ_{hip} (N.m)	τ_{knee} (N.m)	τ_{ankle} (N.m)	GRF _x (N)	GRF _y (N)	R _x (N)	R _y (N)	R _z (N.m)
trajectory optimization	R: 16.46 L: 18.07	R: 11.06 L: 11.18	R: 17.29 L: 17.09	R: 36.42 L: 36.60	R: 234.67 L: 232.46	94.35	349.03	18.12
optimal control	R: 0.42 L: 0.42	R: 0.35 L: 0.35	R: 0.66 L: 0.66	R: 19.81 L: 8.33	R: 26.49 L: 26.38	0	0	0

R_x, R_y and R_z represent the residual forces and torque on the pelvis. R and L refer to right and left legs.

4.2.6 Initial guess

The initial guess for time, states, control inputs and the integrals of the cost terms were set to the data described in Sect. 3 and the initial guess for the contact parameters were set to the contact parameters reported in [5].

5 Results and discussion

Since the number of constraints, variables and cost terms in the optimal control optimization was higher than those in the trajectory optimization, the computation time of optimal control (11 minutes) was longer than that of the trajectory optimization (6 minutes). However, both of our optimizations, in which symbolic dynamic equations are used, are still more computationally efficient than the equivalent optimizations in which numerical dynamic equations are used [26]. The reason is that in our optimizations, differential equations were symbolically calculated only once and then being called in the optimization procedure many times while in the numerical optimizations equivalent, differential equations are re-formulated each time they are called, leading to higher computation time.

The values of weighting factors in the cost functions of both optimizations are shown in Table 6. The weights of motion, torque and GRF tracking terms were set to 1/4 to have the same effects on the results. The weight of the jerk cost term was set to a lower value ($w_4 = 1/40$) to affect the results less since the jerk term is only for convergence and solution smoothness. It should be noted that in Eq. 5 and Eq. 11, the tracking terms were divided by the range of each quantity (i.e., maximum value - minimum value) to be dimensionless and comparable.

The resultant joint torques and GRFs from the trajectory and optimal control optimizations are shown in Fig. 8 and Fig. 9, respectively. The simulated results from the optimal control optimization (second columns in Fig. 8 and Fig. 9) were mostly within the standard deviation of the experimental data. The simulated results from the trajectory optimization (first columns in Fig. 8 and Fig. 9) were not as accurate as the results from the optimal control. The root-mean-square errors (RMSEs) of joint torques and GRFs are shown for trajectory optimization and optimal control in Table 7.

The geometries of the ellipsoids obtained from the trajectory optimization and optimal control are shown in Fig. 10 and Fig. 11, respectively. The geometry information of the left

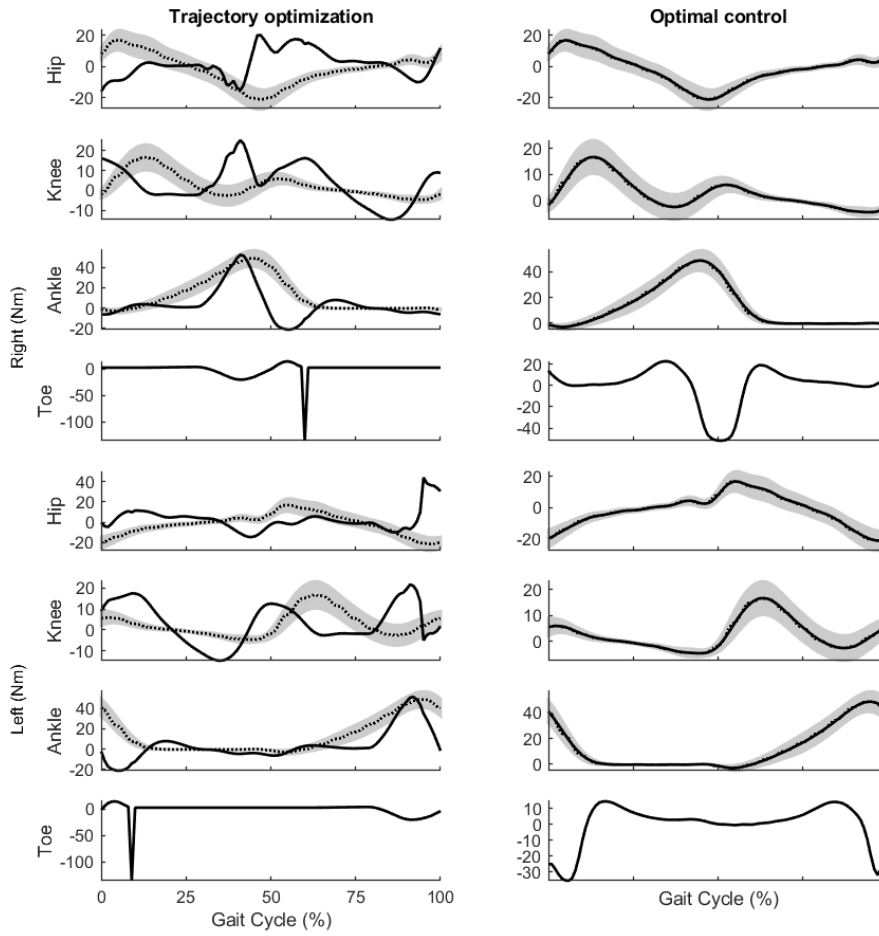


Fig. 8: The lower extremity joint torques from trajectory optimization (first column) and optimal control (second column) (The dotted lines represent the mean experimental torques and the gray areas show the standard deviations of the mean experimental torques reported by [3])

foot, in these two figures, are listed in Tables 8 and 9, respectively. The ellipsoids of the left and right feet have the same dimensions but are bilaterally symmetric. The optimized ellipsoids from the optimal control matched the geometry of the foot better than those from the trajectory optimization.

The remainder of the contact parameters optimized through the trajectory optimization and the optimal control are in Table 10 and Table 11, respectively. Each parameter has different values for the three different ellipsoids due to the complex structure of foot. In particular, the human foot consists of 33 joints, 26 bones, 19 muscles and 107 ligaments

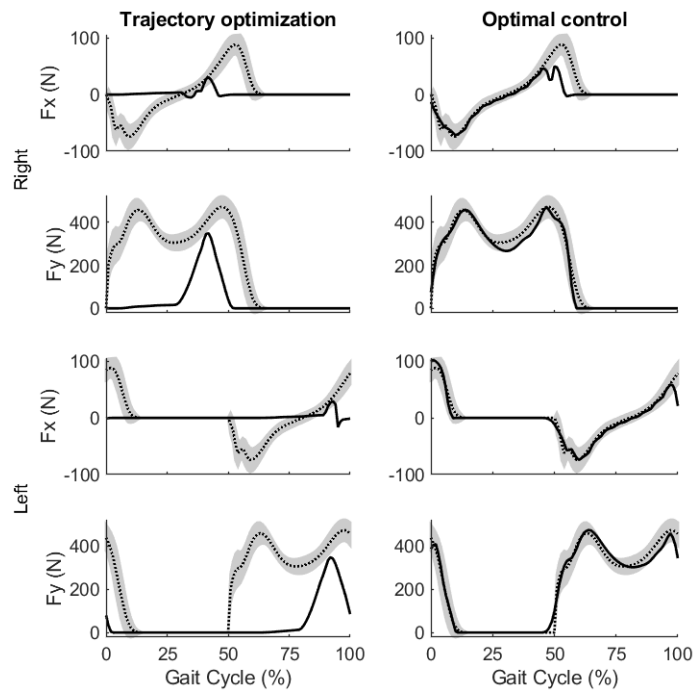


Fig. 9: The tangential and normal ground reaction forces from trajectory optimization (first column) and optimal control (second column) (The dotted lines represent the mean experimental GRFs and the gray areas show the standard deviations of the mean experimental GRFs reported by [3])

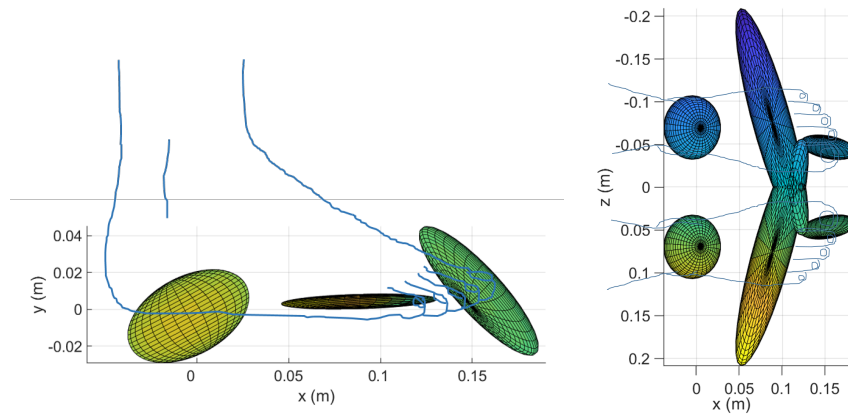


Fig. 10: The optimized contact model geometry from trajectory optimization

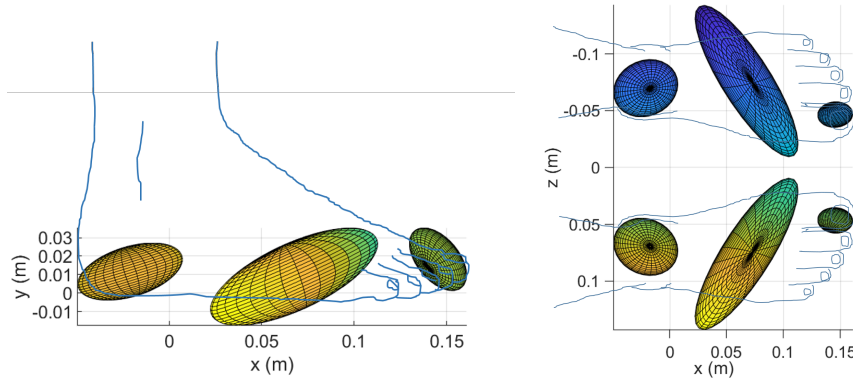


Fig. 11: The optimized contact model geometry from optimal control

Table 8: The optimized geometry parameters for the left foot from trajectory optimization

ellipsoid	dimensions (m)			orientations (degree)			positions (m)		
	a	b	c	γ	β	α	r_x	r_y	r_z
toe	0.0114	0.0464	0.0148	-46.33	-21.37	151.26	0.1535	0.0100	0.0235
ball	0.1377	0.0226	0.0039	-74.61	-3.86	-89.18	0.0882	0.0042	-0.0060
heel	0.0374	0.0358	0.0213	-79.07	-28.26	-91.69	-0.0047	-0.0037	0

Table 9: The optimized geometry parameters for the left foot from optimal control

ellipsoid	dimensions (m)			orientations (degree)			positions (m)		
	a	b	c	γ	β	α	r_x	r_y	r_z
toe	0.0118	0.0200	0.0110	-47.33	-29.48	152.46	0.1454	0.0183	0.0235
ball	0.0800	0.0218	0.0179	-57.03	-17.99	-95.45	0.0675	0.0089	-0.0060
heel	0.0245	0.0300	0.0135	-68.87	-17.18	-91.62	-0.0212	0.0116	0

Table 10: The optimized contact parameters from trajectory optimization

	toe	ball	heel
$k_v(N/m^3)$	1.67e7	1.04e7	0.07e7
$a_v(s/m)$	0.9161	0.6881	1.4732
μ_s	0.0200	0.6256	0.2207
μ_d	0.0139	0.4245	0.1592

surrounded by a tissue and the different sections of this tissue have different mechanical properties (e.g., roughness and thickness).

Since the center of pressure is much closer to the fore-foot than the toe and heel (i.e., the ball ellipsoid is more in contact with the ground than the heel and toe ellipsoid) during gait, the ball ellipsoids play a more important role in generating the normal GRF, and also avoiding slippage, than the toe and heel ellipsoids. The optimal control optimization identified the largest values for the penetration volume and the dynamic friction coefficient of the ball ellipsoids among the ellipsoids (see Fig. 11 and Table 11). Furthermore, the optimal control optimization identified the lowest and greatest values for the volumetric stiffness and damping of the ball ellipsoids, respectively that proves that the ball ellipsoids

Table 11: The optimized contact parameters from optimal control

	toe	ball	heel
$k_v(N/m^3)$	4.60e7	0.12e7	0.95e7
$a_v(s/m)$	0.0654	3.0000	2.1490
μ_s	0.0102	1.2000	0.1765
μ_d	0.0100	1.1871	0.1121

also have a big effect on the smoothness of the normal GRFs, in comparison to the toe and heel ellipsoids.

However, the geometry of the ball ellipsoids, identified in the trajectory optimization, was not as expected. As shown in Fig. 10, the ball ellipsoids did not have an adequate penetration volume to create the normal GRFs. To compensate, the heel and toe ellipsoids had unnatural geometries and large penetration volumes, which did not succeed in generating accurate GRFs.

Another reason behind the inaccurate tangential GRFs from the trajectory optimization would be the methodology used (explicit inverse dynamics simulation). The friction in our foot-ground contact was generated by a continuous velocity-based friction model. It is difficult for a velocity-based friction model to stay in the sticking regime in an inverse simulation, because any small errors in the experimental velocities (measurement or calculation errors) may lead to large errors in the friction force due to the high sensitivity of friction force to velocity [4]. However, our optimal control optimization, which used implicit dynamics simulation, resulted in a small level of error in the velocity and consequently more accurate tangential GRFs. In the implicit dynamic simulation, the error of the velocity can be controlled better than the explicit inverse dynamics simulation since the joint jerks were considered as a control input and minimized as a cost term and joint torques were also assumed as control inputs driving the model.

Optimal control is more suitable than trajectory optimization to identify a large number of parameters because if some experimental data are not available for being tracked, they can be predicted through the optimal control approach. This optimization provides this possibility for us to track not only the torques but also the motions to estimate more reliable and accurate results for the joint angles and torques for which no experimental data were available.

In the optimal control optimization, the states (i.e., motion and its first and second derivatives) and control inputs (i.e., torques and the third derivative of motion) were parameterized and then estimated through the optimization. Therefore, the absence of the experimental angle and torque for the metatarsal joints and experimental GRMs and center of pressure for the feet were compensated by the predictability feature of the direct collocation method. Fig. 12 shows the simulated motion obtained by the optimal control optimization. Since the simulated joint angles and joint torques, for which the experimental data were available, tracked the corresponding experimental data very well, we can say that the optimal control optimization has predicted physiologically meaningful values for the angles and torques of the metatarsal joints, for which no experimental data were available. Predicted metatarsal torques and angles are shown in Fig. 8 and Fig. 3, respectively.

In the trajectory optimization, the inputs (i.e., motion and its first and second derivatives) were the fixed data measured or calculated from experimental results. Thus, since the third derivatives of motion were always fixed, they could not be minimized unlike the optimal control optimization, in which joint jerks were minimized. Moreover, in the trajectory optimization, unlike the optimal control optimization, no boundaries could be

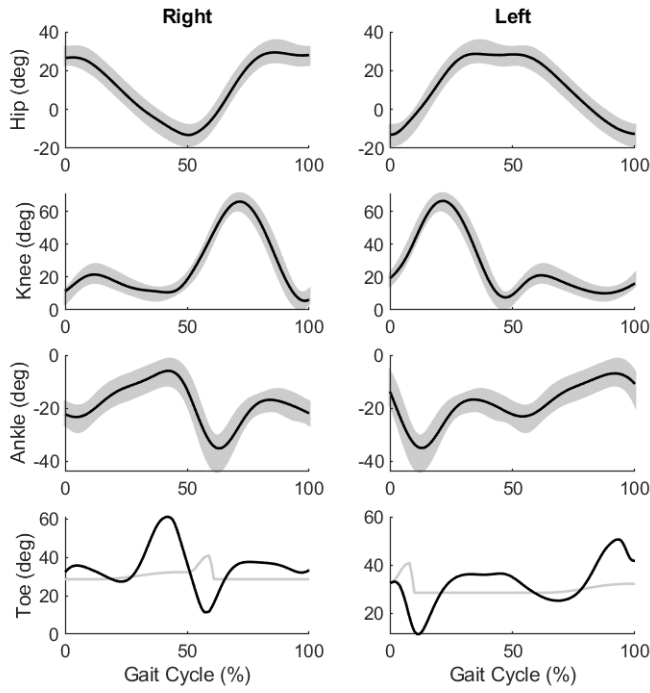


Fig. 12: The lower extremity joint angles from optimal control (The gray areas in the plots of hip, knee and ankle joint angles represent the mean experimental angle data with the specified standard deviations reported by [3] and the gray lines in the plots of metatarsal angles represent the trajectory we planned and considered as the initial guess for the optimization)

defined for the torques and GRFs to lead them to have meaningful values, and also there was no control on the torques that were constrained to satisfy the inverse dynamics.

Another shortcoming of the trajectory optimization is that no path constraints on the outputs could be applied. Therefore, the residual loads on the pelvis could not be reduced to zero thereby causing inaccurate joint torques to be estimated by the optimization. Fig. 13 shows the residual forces and moments obtained by the trajectory optimization and the optimal control optimization; The corresponding RMSEs are shown in Table 7.

6 Conclusion

In this study, a 2D human model was developed and the 3D ellipsoidal volumetric contact was applied on both feet. The dynamic equations of the multibody model and the contact equations were developed symbolically. Two approaches were used to identify the contact parameters: GlobalSearch trajectory optimization and direct collocation optimal control.

The results showed that for parameter identification, especially when not all the experimental data are available, optimal control with implicit dynamics is more accurate

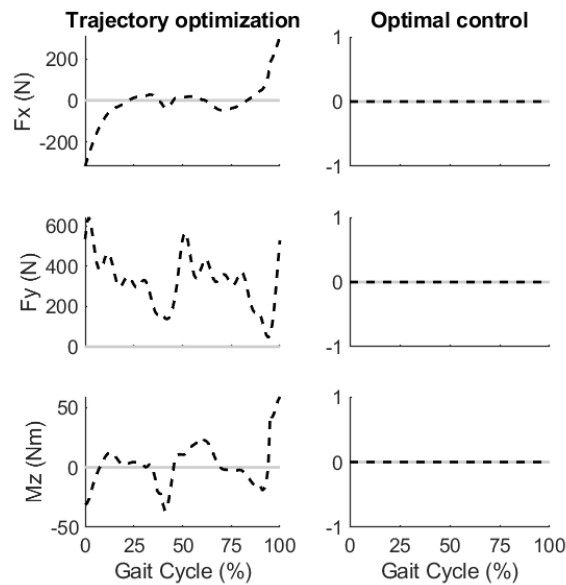


Fig. 13: The residual forces and moment acting on the pelvis obtained from trajectory optimization (first column) and optimal control optimization (second column)

than the trajectory optimization with inverse dynamics. For the optimal control, the root-mean-square errors of the resultant torques, tangential and normal ground reaction forces were 0.48 (N.m), 14.07 (N) and 26.44 (N), respectively. However, for the trajectory optimization, these errors were 15.19 (N.m), 36.51 (N) and 234.57 (N). In addition, we presented a computationally efficient symbolic ellipsoidal volumetric foot-ground contact model that simulates more accurate normal and tangential reaction forces than previous volumetric models [5].

In this study, we could also predict meaningful values for the torques and motions of the metatarsal joints through the optimal control approach. However, we believe that more feasible and accurate prediction could have been achieved if the experimental GRMs and center of pressure for the feet were available.

Our future goal is to use the proposed contact model in a fully-predictive predictive human gait simulation, not only to predict novel motions but also to obtain the motions and torques of metatarsal joints.

Acknowledgements This research was funded by the Natural Sciences and Engineering Research Council of Canada and the Canada Research Chairs program. Special thanks to Marco Rabuffetti and Maurizio Ferrarin from Polo Tecnologico, IRCCS S. Maria Nascente, Fondazione Don C. Gnocchi, Italy for providing us with their gait experimental data.

References

1. Anderson, F.C., Pandy, M.G.: Individual muscle contributions to support in normal walking. *Gait and Posture* **17**(2), 159–169 (2003). DOI 10.1016/S0966-6362(02)00073-5

2. van den Bogert, A.J., Blana, D., Heinrich, D.: Implicit methods for efficient musculoskeletal simulation and optimal control. *Procedia IUTAM* **2**, 297–316 (2011). DOI 10.1016/J.PIUTAM.2011.04.027
3. Bovi, G., Rabuffetti, M., Mazzoleni, P., Ferrarin, M.: A multiple-task gait analysis approach: Kinematic, kinetic and EMG reference data for healthy young and adult subjects. *Gait & Posture* **33**(1), 6–13 (2011). DOI 10.1016/j.gaitpost.2010.08.009
4. Brown, P.: Contact Modelling for Forward Dynamics of Human Motion. Masters thesis, University of Waterloo (2017)
5. Brown, P., McPhee, J.: A 3D ellipsoidal volumetric foot–ground contact model for forward dynamics. *Multibody System Dynamics* **42**(4), 447–467 (2018). DOI 10.1007/s11044-017-9605-4
6. Erdemir, A., Piazza, S.J.: Changes in foot loading following plantar fasciotomy: A computer modeling study. *Journal of Biomechanical Engineering* **126**(2), 237 (2004). DOI 10.1115/1.1691447
7. Ezati, M., Ghannadi, B., McPhee, J.: A review of simulation methods for human movement dynamics with emphasis on gait. *Multibody System Dynamics* pp. 1–28 (2019). DOI 10.1007/s11044-019-09685-1
8. Ezati, M., Khadiv, M., Moosavian, S.: An investigation on the usefulness of employing a two-segment foot for traversing stairs. *International Journal of Humanoid Robotics* **14**(4) (2017). DOI 10.1142/S021984361750027X
9. Fregly, B.J., Bei, Y., Sylvester, M.E.: Experimental evaluation of an elastic foundation model to predict contact pressures in knee replacements. *Journal of biomechanics* **36**(11), 1659–68 (2003). DOI 10.1016/S0021-9290(03)00176-3
10. Geyer, H., Herr, H.: A Muscle-reflex model that encodes principles of legged mechanics produces human walking dynamics and muscle activities. *IEEE Transactions on Neural Systems and Rehabilitation Engineering* **18**(3), 263–273 (2010). DOI 10.1109/TNSRE.2010.2047592
11. Ghannadi, B., Mehrabi, N., Sharif Razavian, R., McPhee, J.: Nonlinear model predictive control of an upper extremity rehabilitation robot using a two-dimensional human-robot interaction model. In: *IEEE/RSJ International Conference on Intelligent Robots and Systems (IROS)*, pp. 502–507. IEEE, Vancouver, British Columbia, Canada (2017). DOI 10.1109/IROS.2017.8202200
12. Gilardi, G., Sharf, I.: Literature survey of contact dynamics modelling. *Mechanism and Machine Theory* **37**(10), 1213–1239 (2002). DOI 10.1016/S0094-114X(02)00045-9
13. Gonthier, Y.: Contact Dynamics Modelling for Robotic Task Simulation. Phd thesis, University of Waterloo (2007)
14. Gonthier, Y., McPhee, J., Lange, C., Piedbœuf, J.C.: A Contact Modeling Method Based on Volumetric Properties. In: *Volume 6: 5th International Conference on Multibody Systems, Nonlinear Dynamics, and Control*, Parts A, B, and C, vol. 2005, pp. 477–486. ASME (2005). DOI 10.1115/DETC2005-84610
15. Grönqvist, R., Abeysekera, J., Gard, G., Hsiang, S.M., Leamon, T.B., Newman, D.J., Gielo-Perczak, K., Lockhart, T.E., Pai, C.Y.: Human-centred approaches in slipperiness measurement. In: *Ergonomics*, vol. 44, pp. 1167–1199. Taylor & Francis Group (2001). DOI 10.1080/00140130110085556
16. Hunt, K.H., Crossley, F.R.E.: Coefficient of restitution interpreted as damping in vibroimpact. *Journal of Applied Mechanics* **42**(2), 440 (1975). DOI 10.1115/1.3423596
17. Koenraadt, K.L., Stolwijk, N.M., van den Wildenberg, D., Duysens, J., Keijsers, N.L.: Effect of a metatarsal pad on the forefoot during gait. *Journal of the American Podiatric Medical Association* **102**(1), 18–24 (2012). DOI 10.7547/1020018
18. Leardini, A., Benedetti, M.G., Berti, L., Bettinelli, D., Nativo, R., Giannini, S.: Rear-foot, mid-foot and fore-foot motion during the stance phase of gait. *Gait and Posture* **25**(3), 453–462 (2007). DOI 10.1016/j.gaitpost.2006.05.017
19. Lim, Y.P., Lin, Y.C., Pandey, M.G.: Effects of step length and step frequency on lower-limb muscle function in human gait. *Journal of Biomechanics* **57**, 1–7 (2017). DOI 10.1016/j.jbiomech.2017.03.004
20. Lin, Y.C., Haftka, R.T., Queipo, N.V., Fregly, B.J.: Surrogate articular contact models for computationally efficient multibody dynamic simulations. *Medical engineering & physics* **32**(6), 584–94 (2010). DOI 10.1016/j.medengphy.2010.02.008
21. Lin, Y.C., Kim, H.J., Pandey, M.G.: A computationally efficient method for assessing muscle function during human locomotion. *International Journal for Numerical Methods in Biomedical Engineering* **27**(3), 436–449 (2011). DOI 10.1002/cnm.1396
22. Lin, Y.C., Pandey, M.G.: Three-dimensional data-tracking dynamic optimization simulations of human locomotion generated by direct collocation. *Journal of biomechanics* **59**, 1–8 (2017). DOI 10.1016/j.jbiomech.2017.04.038
23. Lin, Y.C., Walter, J.P., Pandey, M.G.: Predictive simulations of neuromuscular coordination and joint-contact loading in human gait. *Annals of Biomedical Engineering* **46**(8), 1216–1227 (2018). DOI 10.1007/s10439-018-2026-6
24. Lopes, D.S., Neptune, R.R., Ambrósio, J.A., Silva, M.T.: A superellipsoid-plane model for simulating foot-ground contact during human gait. *Computer Methods in Biomechanics and Biomedical Engineering* **19**(9), 954–963 (2016). DOI 10.1080/10255842.2015.1081181

25. McLaughlin, T., Zourntos, T.: Using Fourier analysis to generate believable gait patterns for virtual quadrupeds. Masters thesis, Texas A&M University (2013)
26. McPhee, J., Wells, C.: Automated Symbolic Analysis of Mechanical System Dynamics. *MapleTech* **3**, 48–56 (1996)
27. Meyer, A.J., Eskinazi, I., Jackson, J.N., Rao, A.V., Patten, C., Fregly, B.J.: Muscle synergies facilitate computational prediction of subject-specific walking motions. *Frontiers in Bioengineering and Biotechnology* **4**, 77 (2016). DOI 10.3389/fbioe.2016.00077
28. Millard, M., McPhee, J., Kubica, E.: Multi-step forward dynamic gait simulation. In: C.L. Bottasso (ed.) *Multibody Dynamics*, pp. 25–43. Springer Netherlands, Dordrecht (2009). DOI 10.1007/978-1-4020-8829-2_2
29. Miller, R.H.: A comparison of muscle energy models for simulating human walking in three dimensions. *Journal of biomechanics* **47**(6), 1373–81 (2014). DOI 10.1016/j.jbiomech.2014.01.049
30. Mouzo, F., Lugris, U., Pamies Vila, R., Font Llagunes, J.M., Cuadrado Aranda, J.: Underactuated approach for the control-based forward dynamic analysis of acquired gait motions. In: *Proceedings of the ECCOMAS Thematic Conference on Multibody Dynamics*, pp. 1092–1100 (2015)
31. Neptune, R.R., Wright, I.C., van den Bogert, A.J.: A method for numerical simulation of single limb ground contact events: Application to heel-toe running. *Computer Methods in Biomechanics and Biomedical Engineering* **3**(4), 321–334 (2000). DOI 10.1080/10255840008915275
32. Patterson, M.A., Rao, A.V.: GPOPS-II. *ACM Transactions on Mathematical Software* **41**(1), 1–37 (2014). DOI 10.1145/2558904
33. Peasgood, M., Kubica, E., McPhee, J.: Stabilization of a dynamic walking gait simulation. *Journal of Computational and Nonlinear Dynamics* **2**(1), 65 (2007). DOI 10.1115/1.2389230
34. Porsa, S., Lin, Y.C., Pandy, M.G.: Direct methods for predicting movement biomechanics based upon optimal control theory with implementation in OpenSim. *Annals of Biomedical Engineering* **44**(8), 2542–2557 (2016). DOI 10.1007/s10439-015-1538-6
35. Rao, A.V.: A survey of numerical methods for optimal control. *Advances in the Astronautical Sciences* **135**(1), 497–528 (2009). DOI 10.1515/jnum-2014-0003
36. Sandhu, S.S., McPhee, J.: A Two-Dimensional Nonlinear Volumetric Foot Contact Model. In: *Volume 2: Biomedical and Biotechnology Engineering*, pp. 703–710. ASME (2010). DOI 10.1115/IMECE2010-39464
37. Sharif Shourijeh, M.: *Optimal Control and Multibody Dynamic Modelling of Human Musculoskeletal Systems* (2013)
38. Sharif Shourijeh, M., McPhee, J.: Forward dynamic optimization of human gait simulations: a global parameterization approach. *Journal of Computational and Nonlinear Dynamics* **9**(3), 031018 (2014). DOI 10.1115/1.4026266
39. Shourijeh, M.S., McPhee, J.: Foot–ground contact modeling within human gait simulations: from Kelvin–Voigt to hyper-volumetric models. *Multibody System Dynamics* **35**(4), 393–407 (2015). DOI 10.1007/s11044-015-9467-6
40. Silva, M., Freitas, B., Andrade, R., Carvalho, Ó., Renjewski, D., Flores, P., Espregueira-Mendes, J.: Current perspectives on the biomechanical modelling of the human lower limb: a systematic review. *Archives of Computational Methods in Engineering* (2020). DOI 10.1007/s11831-019-09393-1
41. Smith, C.R., Vignos, M.F., Lenhart, R.L., Kaiser, J., Thelen, D.G.: The Influence of Component Alignment and Ligament Properties on Tibiofemoral Contact Forces in Total Knee Replacement. *Journal of Biomechanical Engineering* **138**(2), 021017 (2016). DOI 10.1115/1.4032464
42. Sun, J., Voglewede, P.A.: Dynamic simulation of human gait using a combination of model predictive and PID control. In: *Volume 6: 10th International Conference on Multibody Systems, Nonlinear Dynamics, and Control*, p. V006T10A008. ASME (2014). DOI 10.1115/DETC2014-35582
43. Sun, J., Wu, S., Voglewede, P.A.: Dynamic simulation of human gait model with predictive capability. *Journal of Biomechanical Engineering* **140**(3), 031008 (2018). DOI 10.1115/1.4038739
44. Ugray, Z., Lasdon, L., Plummer, J., Glover, F., Kelly, J., Martí, R.: Scatter Search and Local NLP Solvers: A Multistart Framework for Global Optimization. *INFORMS Journal on Computing* **19**(3), 328–340 (2007). DOI 10.1287/ijoc.1060.0175
45. Umberger, B.R.: Effects of suppressing arm swing on kinematics, kinetics, and energetics of human walking. *Journal of Biomechanics* **41**(11), 2575–2580 (2008). DOI 10.1016/j.jbiomech.2008.05.024
46. Winter, D.A.: *Biomechanics and motor control of human movement*. Wiley (2009)
47. Zmitrowicz, A.: Contact stresses: a short survey of models and methods of computations. *Archive of Applied Mechanics* **80**(12), 1407–1428 (2010). DOI 10.1007/s00419-009-0390-2